

# Kinetic and Thermodynamic Study on the Removal of Congo Red from the Aqueous Solution Using Graphene Oxide/Magnesium Oxide Nanocomposite

Amir Fahdil, Dawood AL-Niimi, Firas Hassan Muhi\*

Received: 12 May 2019 / Received in revised form: 04 October 2019, Accepted: 12 October 2019, Published online: 27 December 2019  
© Biochemical Technology Society 2014-2019  
© Sevas Educational Society 2008

## Abstract

In this investigation, graphene oxide/magnesium oxide (GO/MgO NCs) Nanocomposite with GO/MgO weight ratio of 1:1 was used to removal Congo red dye from aqueous solution in batch method. The prepared NCs were characterized using scanning electron microscopy, X-ray diffraction, FTIR, Atomic force microscope, and Brunauer, Emmett and Teller (BET). The results showed that MgO particles were successfully grafted on GO. The effects of different empiric variables on the Congo red dye removal including GO/MgO NCs weight, initial concentration, contact time, and pH were investigated. The experimental analysis of adsorption isotherms (Langmuir, Freundlich, Dubinin, Temkin) indicated that adsorption data were best fit with the Freundlich isotherm model. The kinetic adsorption data were best expressed by the pseudo-second-order kinetic model. Thermodynamic function data such as ( $\Delta H^\circ$ ,  $\Delta G^\circ$ ,  $\Delta S^\circ$ ) of adsorption were calculated, which showed the adsorption exothermic process and the value of  $\Delta G^\circ$  was negative and indicated that the process happened spontaneously while the value of  $\Delta S^\circ$  was positive, meaning that the movements of dye molecules is unlimited.

**Key words:** Adsorption, Congo red, GO/MgO NCs, Thermodynamic and Kinetic Study

## Introduction

The influx of dyes in the environment is troubling for both toxicological and aesthetical reasons (Farhan et al., 2018; Mahmoud et al., 2018). Industry such as plastics, texture, paper, lacing, etc. are some of the sources for dye waste water (Mahmoud et al., 2019) approaching ten thousand different dyes and tincture are produced annually worldwide and used extensively within the food, pharmaceutical, textile, cosmetics, leather, and printing industries. It is calculable that between ten and two hundreds of regarding  $7 \times 10^5$  heaps of coloring material being factory-made every year and utilized in coloring processes are also found in waste material (Soares et al., 2001). Dye waste material is usually characterized by high salt and organic content and low biodegradation potential. Waste materials containing dyes are also carcinogenic and toxic and are a serious danger to aquatic organisms (Robinson et al., 2001; Mohan et al., 2002; Bakhy 2018). A popular way to treat dye effluents embraces

surface assimilation (Harja et al., 2011). Surface assimilation is growing in quality thanks to its benefits of the straight forward operation, low cost, fast treatment, and effectiveness for removing low dye concentration of waste streams (Alpat et al., 2008). The advantages of sorption area unit its clarity of operation, low prices (compared to alternative separation processes). (Oakes and Dixon 2003; Alseroury 2018). Liquid-phase adsorption is effectively used for removing dye from wastewater. (Wu et al., 1998). Adsorption is a widely-used method for treating industrial wastewaters containing colors, heavy metals, and other inorganic and organic impurities (Rawnaq et al., 2018; Allen et al., 2004; Walker et al., 2003). Congo Red is a model compound for a common soluble group of dyes, which is employed in dyes, textile, plastic, and paper industries (Sponza and Isik, 2005). Dye is an organic material that is able to impart specific colors to the substance used. There is a spread of dyes including acid dyes, basic dyes, azo dyes, mordant dyes, plastic dyes, etc. (Yousefi et al., 2011). The present study the surface assimilation of Congo red dye from its binary compound solutions by GO/MgO NCs.

## Experimental

**Instruments:** The pH of the solutions was measured by pH meter (7110 (WTW), Germany). UV-Visible (Shimadzu, Japan 1700) was utilized to measure dye concentration in the aqueous solution. The temperature was checked using an isothermal bath shaker (BS-11, Korea). The Nanocomposites were determined by XRD (Shimadzu company (Japan) (XRD-6000)) with Cu  $\alpha$  radiation ( $\lambda = 0.1540$  nm). (The measurement condition of XRD was 30 mA, 40 kV, the scanning range and speed was 10-120° and 5 deg/min, respectively), FTIR (Shimadzu, IR PRESTIGE 21) with the KBr pellet technique. 400-4000  $\text{cm}^{-1}$  was the efficient range. SEM (Type Tescan Brno-Mira 3LMU). AFM (SPM-AA3000, Advanced Angstrom Inc.). All chemicals were used with no further purification.

### GO Preparation

The GO was prepared in accordance with the modified Hummers method (Tavakoli et al., 2015). In summary, 2 g graphite powder was mixed with 2g sodium nitrate and 50 ml sulfuric acid (98 wt%) in a 500-mL flask in an ice bath at 0°C. While strongly stirring, 6g potassium permanganate was gradually added into the flask and stirring was kept for 2 hours. Then, 100 ml of deionized (DI) water was poured to the solution; the solution temperature quickly increased to 98 °C and kept at this temperature for 0.5 h.

Amir Fahdil, Dawood AL-Niimi, Firas Hassan Muhi\*

Department of Chemistry, College of Science, University of Diyala, Diyala, Iraq.

\*Email: amansouri @ kau.edu.sa

Then, 300ml DI water was added up to the flask. Following that, 20 ml H<sub>2</sub>O<sub>2</sub> (30 wt %) solution was added and led to changing the color of the mixture to yellow. The mix was filtered and washed with hydrochloric acid (5 %) solution and deionized water sundry times to rest any residuals. Eventually, GO was synthesized by sonication of the dispersal for 1 h and drying at 60°C.

#### Synthesis of MgO NPs

The preparation of MgO NPs was as follows. 2.06 g citric acid was and 2 g MgCl<sub>2</sub>.6H<sub>2</sub>O were separately dissolved in 25 ml DI water in a 250-ml flask. The two solutions were mixed by the slow addition of the MgCl<sub>2</sub>.6H<sub>2</sub>O solution to the citric acid solution with string. Then, some drops of ammonia were slowly added to reach pH 7. After that, the temperature rose to 60°C with stirring for 1h to configure the magnesium hydroxide. Then, the solution was centrifuged for the separation of Mg(OH)<sub>2</sub> gel from the suspension. Mg(OH)<sub>2</sub> gel was eluted 2-3 times with DI water and calcination was conducted at 550 °C for 2h.

#### Synthesis of GO/MgO NCs

The nanocomposite was prepared by combining oxidine in a ratio of 1:1 so that 1g nanoGraphine oxide was weighed and dissolved in 50 ml ionic water in a 250-ml beaker and then, 1g nanomagnetic oxide was dissolved in 50 ml ionic water in another 250-ml beaker. After that, the content of the first beaker was slowly added into the second one with continuous stirring and then the solution was placed in the ultrasound machine and dried at 60°C.

#### Synthesis of Congo red dye solution

Congo red dye is water-soluble ( $\lambda$  max = 497nm). A standard solution (1000 mg/L) was made by dissolving 1g Congo red dye in 1L of DI water. The working solution was made by diluting the standard dye solution with DI water to reach the desired concentration of the solutions (10-50 ppm) and the solutions were left for 24 h to homogenize. Dilute HCl (0.1 M) and NaOH (0.1 M) were used for pH modification. The calibration curve for Congo red dye ( $\lambda$  max = 497nm) was determined by UV-Visible spectrometer. The dye adsorption by a batch process was studied different parameters such as contact time (10-50 min), the dose of GO/MgO NCs adsorbate (0.01-0.05g), pH (3-12), the concentration of dye (10-50 ppm), and temperature (20-40°C). The samples were shaken and kept for 20 min and then they were filtered in a centrifuge at 3500 rpm for 15 min and filtered using filter paper again and analyzed spectrophotometrically. The following equation (% Adsorption) was used to determine the % of dye adsorption from the aqueous solution (AL-Niaini **et al.**, 2018).

$$\% \text{ Adsorption} = \frac{C_0 - C_e}{C_0} \times 100 \quad (1)$$

where C<sub>0</sub> is the initial concentration of dye solution (mg/L) and C<sub>e</sub> is the final concentration (mg/L) after the adsorption.

The adsorption capacity (Q<sub>e</sub> (mg/g)) was calculated using the following equation.

$$Q_e = \frac{C_0 - C_e}{m} \times V_{sol} \quad (2)$$

**Q<sub>e</sub>**: The amount of solute adsorbed per unit weight of adsorbent (mg/g). **C<sub>e</sub>**: Equilibrium concentration of the solute (mg/L). **V<sub>sol</sub>**: The solution volume (L). **m**: The adsorbent weight (g).

## Results and Discussion

In our previous work, the GO/MgO NCs were well characterized using FTIR, XRD, SEM, and AFM (Amir. and Abdulilah. 2019). The properties of the surface area were evaluated through the adsorption of nitrogen at 77K, which is the temperature equilibrium between the vapor and liquid phases. The resulting surface area for GO/MgO nanoparticles was 32/3736 m<sup>2</sup>/g.

#### Determination of the Equilibrium Time of adsorption

Several adsorption experiments in the contact time range of 10-50 min were performed (figure1). The removal rate of dye onto GO/MgO gradually increased increasing contact time from 10 to 50 min and then remained constant with further increase in contact time. Therefore, a period of twenty minutes of equilibrium was selected for the next studies. At an early stage, dye quickly interacted with many available active sites on the GO/MgO surface, resulting in the fast adsorption. The increase of the contact time gradually reduced the available active sites and weakened the driving force, resulting in a slow adsorption and a longer time to attain the adsorption balance.

#### Adsorbent Weight

The impact of adsorbent on the removal % of dye was examined by taking different quantities of GO/MgO ranging from 0.01 to 0.05 g. The results proved that the best removal capability was obtained at 0.02 g (Figure 2).

#### Effect of pH

The effect of pH was studied in which five samples with the same concentration were separately mixed with 0.02 g GO/MgO and shaken for the same time duration and at an equal pH. After that, the absorbance measured and its percentage was calculated. Figure 3 shows that the adsorption capacity was maximum at pH 8 and decreased with increasing pH. The point of zero charge (pH<sub>pzc</sub>) of GO/MgO NCs was 10.5 and the best pH was 8 for removal dye below pH<sub>pzc</sub> so, for other adsorption mechanisms between dye and GO/MgO NCs including hydrogen bonding and  $\pi$ - $\pi$  interaction addition to the electrostatic attraction.

#### Effect of dye concentration on adsorption

It is important to study the efficiency of GO/MgO NCs adsorption for different initial Congo Red concentrations. The CR concentrations of 10 - 50 ppm were prepared and the performance of dye removal was studied at a pH of 8 after 20 minutes. The best removal efficiency was at 10 ppm (Figure 4).

#### Adsorption Kinetics

In order to investigate the rate of the adsorption process, two most common kinetic models: pseudo-second-order and pseudo-first-order equations were used for the analysis of the experimental data for GO/MgO at an initial CR of 10 ppm (Chia et al., 2013).

$$\ln (q_e - q_t) = \ln q_e - k_1 t \quad (3)$$

$$t / q_t = 1 / k_2 q_e^2 + (1 / q_e) t \quad (4)$$

where  $q_t$  and  $q_e$  (mg/g) are the adsorbed dye amounts at time  $t$  and equilibrium, respectively;  $k_1$  and  $k_2$  are the rate constants of pseudo-first-order ( $\text{min}^{-1}$ ) and pseudo-second-order ( $\text{g/mg}\cdot\text{min}$ ). The plots of the equations were evaluated for best fit by the comparison of their correlation coefficients ( $R^2$ ). Figures 5 and 6 show the straight plots of  $\ln (q_e - q_t)$  vs.  $t$  and  $t/q_t$  vs.  $t$ , respectively. The correlation coefficients of the linear curves of both kinetics show that the process is more likely to follow second-order kinetics. The pseudo-second-order model assumes that the rate-limiting step involves the adsorbate's chemical adsorption on the adsorbent. The adsorption rate constant was calculated for each model by fitting the experimental data (Fig. 5 and 6, and Table 1). As proved by the obtained higher regression coefficient ( $R^2$ ), the kinetics data were corroborated with the pseudo-second-order. Moreover, the calculated values of  $q_e$  for the pseudo-second-order are highly matched with the experimental data much better than those of the pseudo-first-order model, indicating that the adsorption kinetics of dye on GO/MgO was not diffusion-controlled (Toor and Jin 2012).

#### Adsorption Isotherm

In this study, (Langmuir, Freundlich, Temkin, and Dubinin-Kaganer-Radushkevich) isotherms were applied to the batch adsorption experimental data to explain the dye-NCs (GO/MgO) interaction. Langmuir isotherm model assumed the monolayer coverage of the adsorbate on a homogenous adsorbent surface, (Fungaro et al., 2011). The experimental adsorption data were applied to the empirical Langmuir isotherm.

$$C_e / Q_e = 1 / q_{\max} K_L + C_e / q_{\max} \quad (5)$$

Where  $C_e$  is the equilibrium concentration of dye (mg/L);  $q_{\max}$  and  $Q_e$  are the maximum adsorption capacity corresponding to complete monolayer coverage on the surface (mg/g) and the capacity at equilibrium (mg/g), respectively; and  $K_L$  is Langmuir constant (L/mg) related to the energy of sorption. The linear relationship of ( $C_e / Q_e$ ) versus ( $C_e$ ) gives a straight line of slope  $1 / q_{\max}$  and intercept ( $1 / K_L q_{\max}$ ) (Figure 7; Table 2). For the Langmuir model, the maximum adsorption ( $q_{\max}$ ) was negative,

which shows the inadequacy of this model to explain the adsorption process, though it shows good linearity in comparison to other models (Alshabanat et al., 2013). A dimensionless constant separation factor of Langmuir isotherm (RL) was also calculated using the following equation (Gan et al., 2015):

$$RL = 1 / (1 + K_L C_o) \quad (6)$$

Table (2) explains the relationship between RL and natural adsorption.

The Freundlich model is a case for multilayer adsorption and adsorption on heterogeneous surface energies, and it gives an exponential distribution of the active sites. The linear form of this model is represented by:

$$\ln Q_e = \ln K_F + 1/n \ln C_e \quad (7)$$

The Freundlich constants  $K_F$  and  $n$  indicate the adsorption capacity and the adsorption intensity are calculated from the intercept and slope of plot  $\ln Q_e$  versus  $\ln C_e$ , respectively (Figure 8). The adsorption intensity ( $n$ ) showed low values ( $n < 1$ ); this indicates a very low affinity between adsorbents and adsorbate (Fungaro et al., 2011). The Freundlich constant ( $K_F$ ) decreases with increasing the temperature and this is an indication for an exothermic reaction. The Dubinin-Kaganer-Radushkevich (DKR) isotherm, which can give the mechanism of adsorption and energy of adsorption process, is expressed as a linear form (Mall et al., 2006):

$$\ln q_e = \ln q_{\max} - \beta \epsilon^2 \quad (8)$$

where  $q_e$  is the adsorption quantity of Congo red ( $\text{mmol g}^{-1}$ ) and  $q_{\max}$ ,  $\epsilon$ , and  $\beta$  are the DKR single-layer adsorption capacity ( $\text{mmol g}^{-1}$ ), and Polanyi potential ( $\text{J mol}^{-1}$ ), adsorption energy constant ( $\text{mol}^2 \cdot \text{J}^{-2}$ ), respectively.  $\epsilon$  can be represented as follows:

$$\epsilon = RT \ln (1 + 1/ce) \quad (9)$$

$\beta$  and  $q_{\max}$  was derived from the plot of  $\ln q_e$  vs.  $\epsilon^2$ . The adsorption energy  $E$ , ( $\text{J}\cdot\text{mol}^{-1}$ ) was calculated using the equation (10):

$$E = (2\beta)^{-0.5} \quad (10)$$

If the values of  $E$  are below 8 KJ/mol, the mechanism may be a physical adsorption, while  $E$  values between 8-16 KJ/mol assume the adsorption to be controlled by ion exchange and  $E$  more than 16 KJ/mol presume a particle diffusion mechanism (chemical process). It can be observed that the  $E$  value may be physical (electrostatic nature).

Temkin isotherm has 1 factor that shows the interaction between adsorbing particles and adsorbent so vividly. This model was applied in forms, given as eqn:

$$Q_e = B n k_T + B \ln C_e \quad (11)$$

$$B = RT/b \tag{12}$$

By plotting  $q_e$  against  $\ln c_e$  gave the constants,  $KT$  and  $B$ , which are the Temkin isotherm is related heat of adsorption (J/mol) [32]. Constant  $KT$  is equilibrium binding constant (L/mg),  $R$  is the gas constant (8.314J/ mol.k). Adsorption Temkin graph of  $q_e$  against  $\ln c_e$  is plotted (Figure 10) and its calculated parameters ( $B$ ,  $KT$ ) can be seen in Table 3. The dye was followed Freundlich isotherm, Freundlich and Dubinin-Radushkevich adsorption isotherms of the adsorbents by linear analysis; Table 3 summarizes the corresponding isotherm parameters and their correlation coefficients ( $R^2$ ) for each parameter. According to the  $R^2$  for each of the parameters in Table 3, the Freundlich model fitted the experimental data best by linear analysis, whereas the Langmuir fitted worst (Gan et al., 2015).

*Thermodynamic parameters*

Thermodynamic parameter, change in free energy ( $\Delta G^\circ$ ), enthalpy ( $\Delta H^\circ$ ), and entropy ( $\Delta S^\circ$ ) were calculated using the following equation:

$$KC = Ae^{-\Delta H/RT} \tag{13}$$

$$\ln X_m = -\Delta H/RT + K \tag{14}$$

where  $\ln X_m$  is the natural logarithm for greatest amount adsorbed (mg/g),  $K$  is the constant of Van't Hoff equation,  $R$  is the universal gas constant (8.314.10<sup>-3</sup> kJ/mol. K<sup>-1</sup>), and  $T$  is the temperature (Kelvin).

$$\Delta G^\circ = - RT \ln K \tag{15}$$

$$K = Q_e \times m/C_e \times V$$

$$\Delta G^\circ = \Delta H - T\Delta S^\circ \tag{16}$$

$$\Delta S^\circ = \Delta H - \Delta G^\circ / T \tag{17}$$

$\Delta H^\circ$  and  $\Delta S^\circ$  were obtained from the slope and intercept of a Van't Hoff plot of  $\ln K_c$  versus  $1/T$  (Figure 11, Table 4). The thermodynamic parameters were obtained and the negative value of  $\Delta H^\circ$  was an indication of the exothermic nature of the adsorption. The value of  $\Delta G$  is negative showing that the adsorbent could happen spontaneously and the value of  $\Delta S$  is positive, which means the motion of the molecules is not limited (Hacıyakupoglu et al., 2015; Amir and Abduliah 2018).

**Conclusion**

The results obtained showed that (GO/MgO) is an efficient sorbent in removing Congo red dye from the aqueous solutions of Congo red dye on GO/MgO. Thermodynamic studies show that the adsorption process is exothermic and spontaneous, while the value of  $\Delta S$  is positive meaning that the movement of molecules is confined. Adsorption kinetics followed the pseudo-second-order kinetics' rate expression. Isotherms with biter fit to Freundlich isotherm, Freundlich constant ( $kF$ ) decreases with increasing the temperature and this is an indication of exothermic. According to the DKR isotherm, the energy equation gives us a perception of the adsorption mechanism, and  $E < 8KJ/mol$  indicates that the physical force influence.

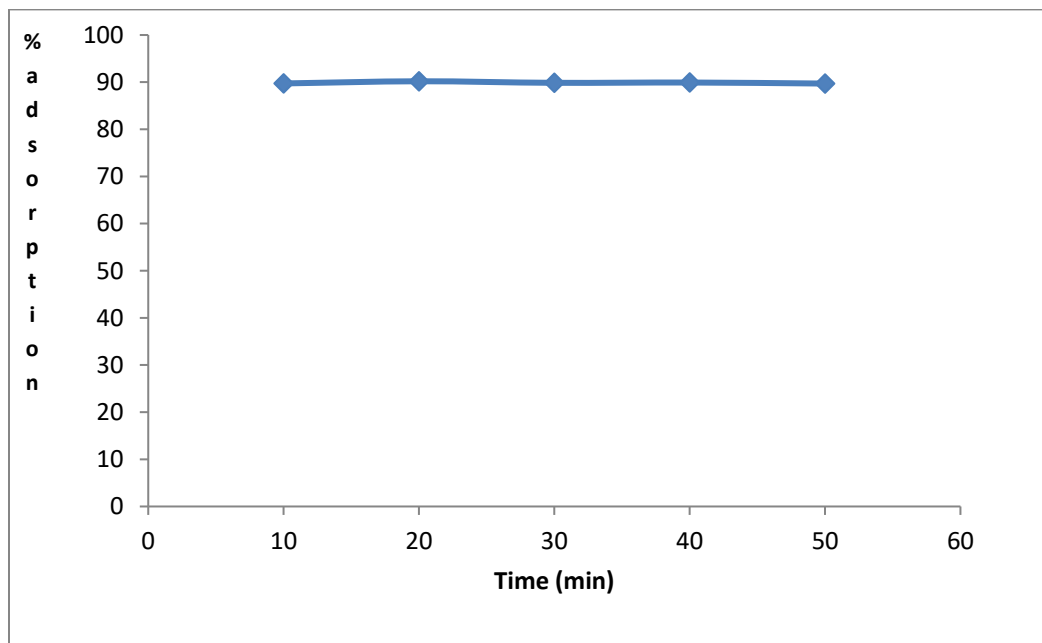


**Figure 1:** Effect of equilibrium time on the Congo red dye adsorption on GO/MgO nanoparticles at 25°C,  $C_o= 30$  ml of 10 ppm, the dose of 0.02 g, and pH=7.

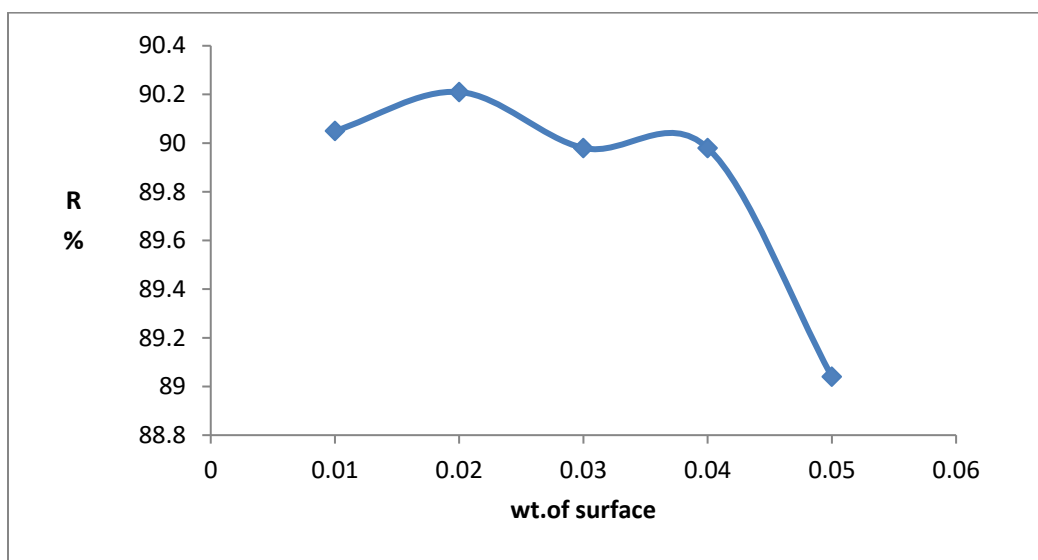


**Figure 2:** Effect of Adsorbent Weight on removal % of Congo Red

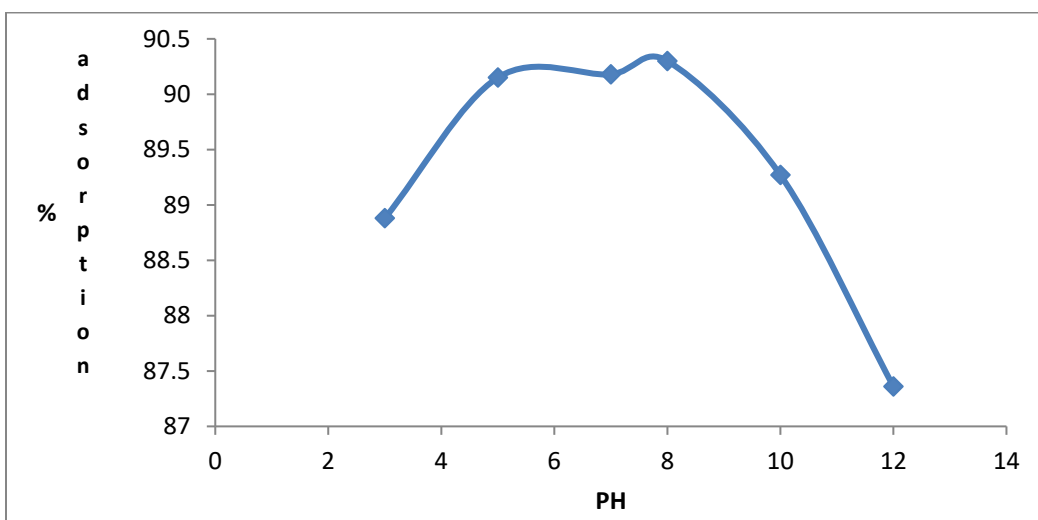


**Figure 3:** Effect of pH on the adsorption of Congo red dye on GO/MgO nanoparticles at 25 °C

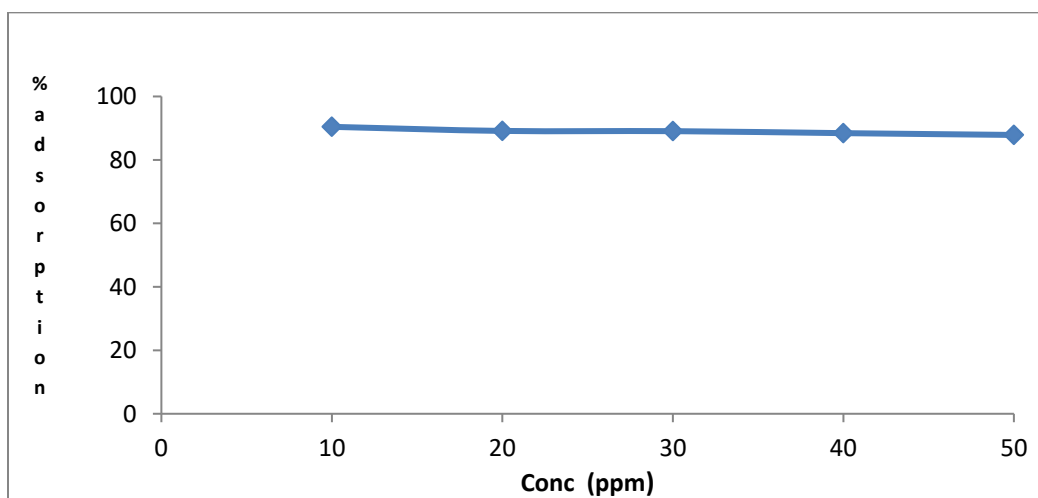


**Figure 4:** Effect of dye concentration on adsorption of Congo red dye on GO/MgO nanoparticles

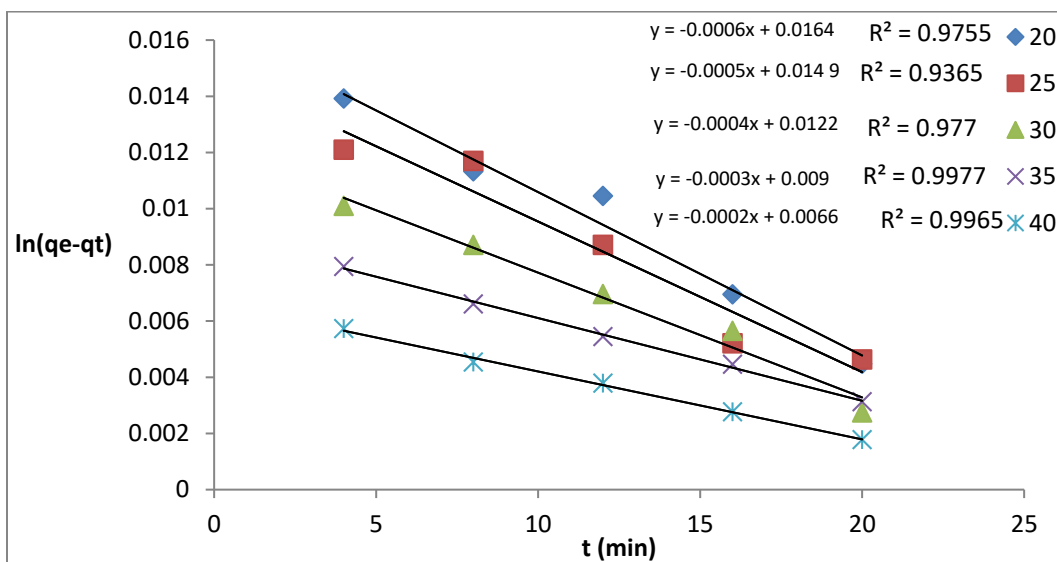


Figure 5: plot of the pseudo-first-order model of Congo red dye on GO/MgO NCs

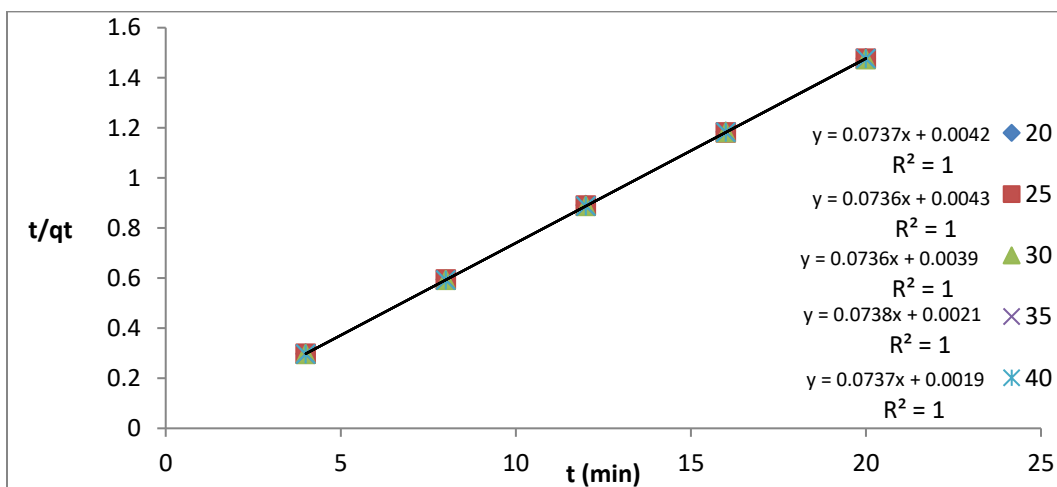


Figure 6: Plot of the pseudo-second-order model of Congo red dye on GO/MgO NCs

Table 1: Kinetics parameters for adsorption Congo red dye on GO/MgO NCs

C <sub>0</sub>	pseudo-first-order					pseudo-second-order		
	T (°C)	q <sub>e</sub> (exp.)	q <sub>e</sub> (calc.)	K1 min <sup>-1</sup>	R <sup>2</sup>	q <sub>e</sub> calc.	K2 g.mg <sup>-1</sup> min <sup>-1</sup>	R <sup>2</sup>
10 ppm	20	13.62	1.016	0.0006	0.975	13.62	1.293	1
	25	13.61	1.015	0.0005	0.936	13.61	1.259	1
	30	13.60	1.012	0.0004	0.977	13.60	1.388	1
	35	13.59	1.009	0.0003	0.997	13.59	2.593	1
	40	13.57	1.006	0.0002	0.996	13.57	2.858	1

Table 2- Values of RL and type of isotherm.

Value of RL	RL >1	RL = 1	RL <1	RL = 0
Type of isotherm	Unfavorable	Linear	Favorable	Irreversible

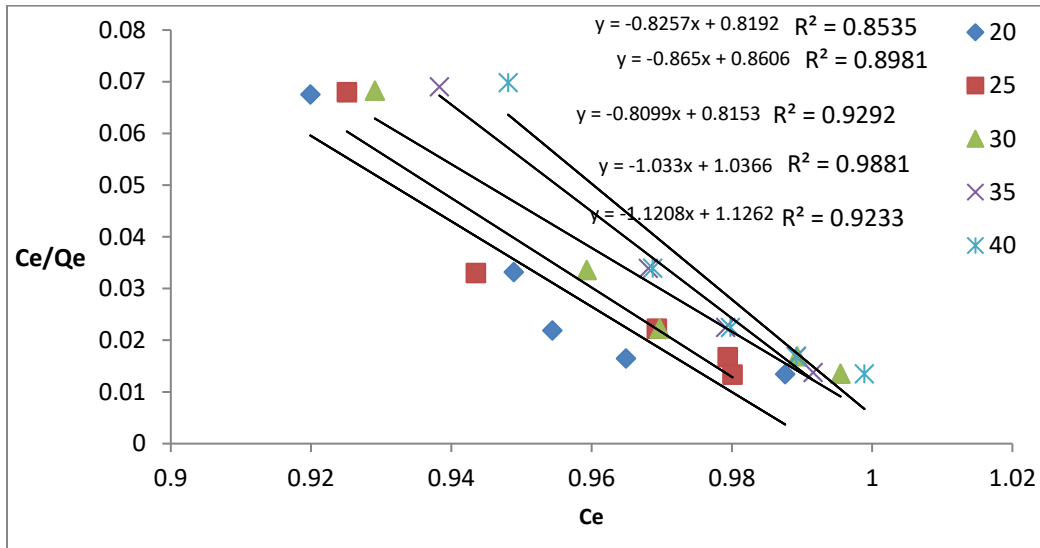


Figure 7: Isotherm Langmuir for Congo red dye on GO/MgO nanoparticles

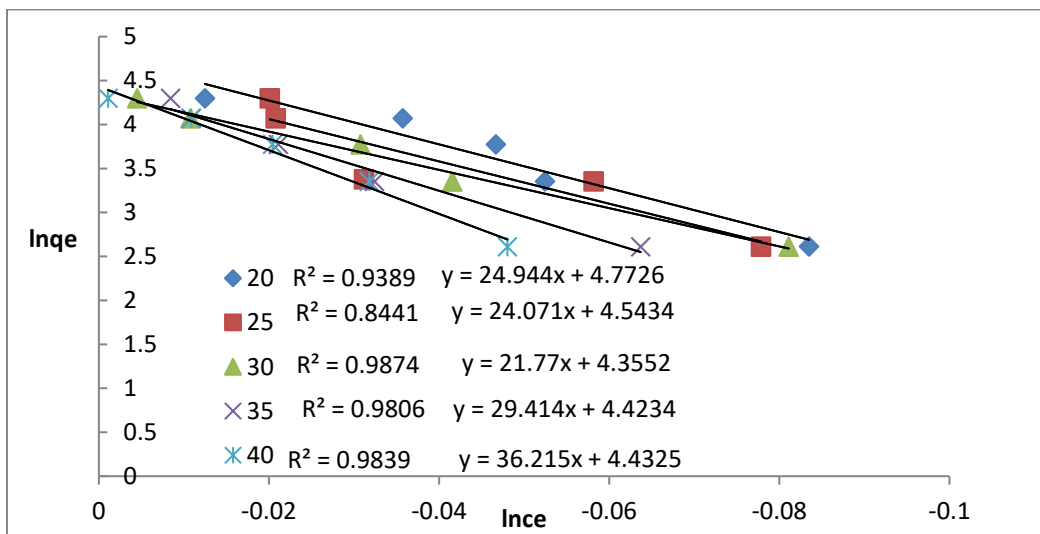


Figure 8: Isotherm Freundlich for Congo red dye at 25°C on GO/MgO nanoparticles.

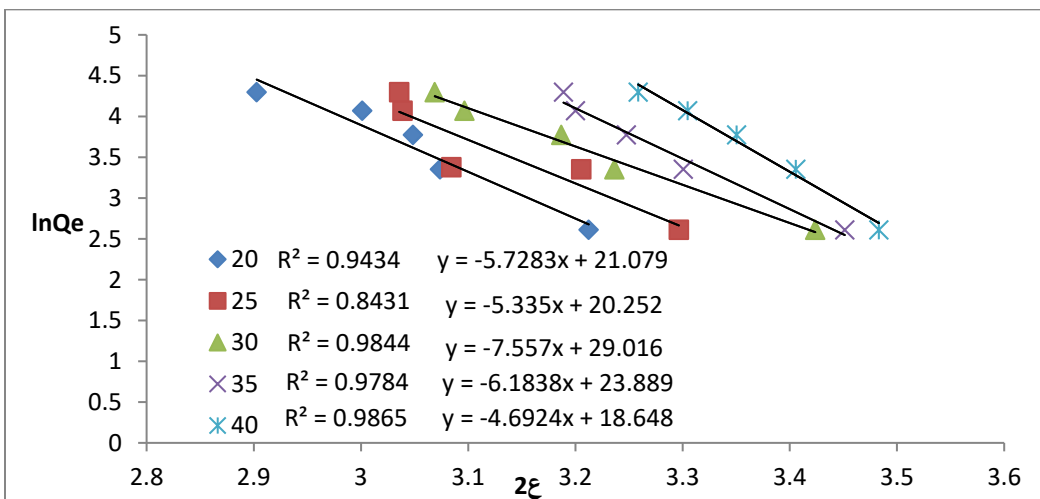


Figure 9: Isotherm Dubinin (DKR) for Orange G dye on GO/MgO NCs

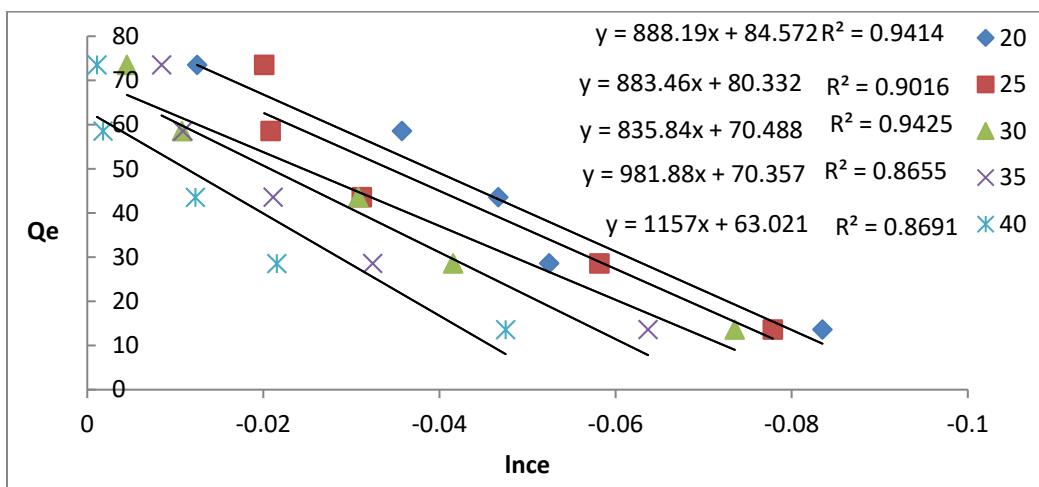


Figure 10: Isotherm Temkin for Congo red dye on GO/MgO NCs

Table 3- The calculated adsorption parameters of the four used isotherms

T(C°)	Langmuir				Freundlich		
	KL	R <sup>2</sup>	q <sub>max</sub>	RL	R <sup>2</sup>	n	K <sub>f</sub>
20	-1.0080	0.8535	-1.211	-0.110	0.9389	0.04009	118.22
25	-0.7445	0.8981	-1.560	-0.155	0.8441	0.04154	94.009
30	-0.9926	0.9292	-1.234	-0.112	0.9874	0.04593	77.88
35	-0.9965	0.9881	-0.968	-0.115	0.9806	0.03399	83.37
40	-0.9962	0.8757	-0.818	-0.111	0.9954	0.03033	81.02

(DKR)				Temkin		
R <sup>2</sup>	E	q <sub>max</sub>	β	KT	B	R <sup>2</sup>
0.9434	3.384	21.079	5.728	84.572	888.19	0.9414
0.8431	3.266	20.252	5.335	80.332	883.46	0.9016
0.9865	3.063	18.648	4.692	70.488	835.84	0.9425
0.9784	3.516	23.889	6.183	70.357	981.88	0.8655
0.9964	3.686	26.493	6.794	63.021	115.70	0.8691

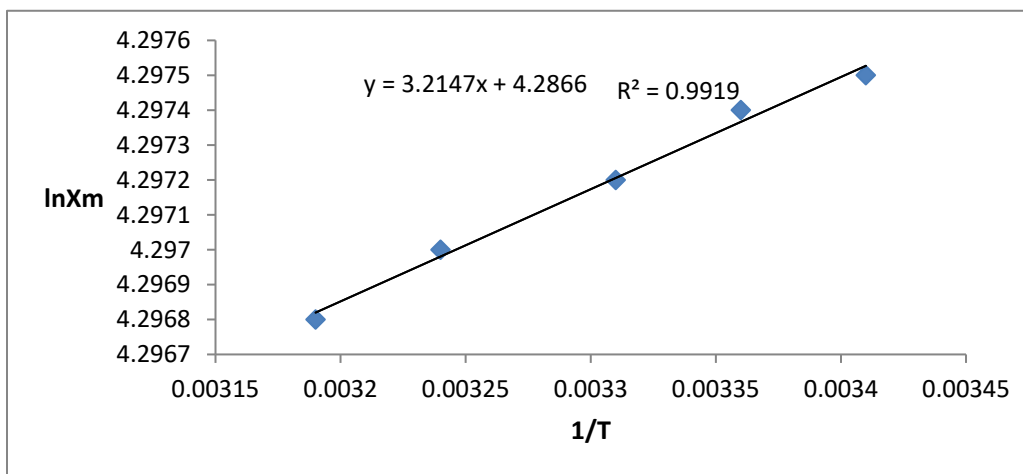


Figure 11: Values of the greatest amounts adsorbed (ln X<sub>m</sub>) for Congo red dye on GO/MgO nanoparticles at different temperatures.



**Table 4:** Values of thermodynamic functions for adsorption Congo red dye on GO/MgO nanoparticles

Ce (mg/L)	Thermodynamic function	20 °C	25 °C	30 °C	35 °C	40 °C
50 ppm	$\Delta H$ kJ.mol <sup>-1</sup>	-0.0267				
	$\Delta G$ kJ.mol <sup>-1</sup>	-10.499	-10.666	-10.822	-10.975	-11.127
	$\Delta S$ J.mol <sup>-1</sup> K <sup>-1</sup>	0.03574	0.03570	0.03562	0.03554	0.03546

## References

- Allen, S. J., McKay, G., & Porter, J. F. (2004). Adsorption isotherm models for basic dye adsorption by peat in single and binary component systems. *Journal of colloid and interface science*, 280(2), 322-333.
- AL-Niaimi, A. F. D., Atiya, G. I., & Abdulateef, D. A. (2018). Thermodynamics and kinetic study of Eosin dye adsorption on CuO nanoparticles. *International Journal of Research in Pharmacy and Chemistry*; 8(2):281-293.
- Alpat, S. K., Özbayrak, Ö., Alpat, Ş., & Akçay, H. (2008). The adsorption kinetics and removal of cationic dye, Toluidine Blue O, from aqueous solution with Turkish zeolite. *Journal of hazardous materials*, 151(1), 213-220.
- Alseroury, F. A. (2018). The Effect of Using Photocatalytic to Decontaminate Wastewater in Natural Sunlight Exposure. *International Journal of Pharmaceutical Research & Allied Sciences*, 7(3).
- Alshabanat, M., Alsenani, G., & Almufarj, R. (2013). Removal of crystal violet dye from aqueous solutions onto date palm fiber by adsorption technique. *Journal of Chemistry*, 1-6.
- Amir.Fahdil.DawoodAL-Niaimi and Abdulilah.Ahmed.Olaiwy (2018). Adsorption of Orange G dye from aqueous solutions using Magnesium oxide Nanoparticles. *J.Biochem Tech* 9(3): 31-38.
- Amir.Fahdil.DawoodAL-Niaimi and Abdulilah.Ahmed.Olaiwy(2019). Removal Orange G dye from aqueous solutions using Graphene oxide/Magnesium oxide Nanocomposite. *International Journal of research in pharmacy and chemistry* 9(1),1-16.
- Bakhy, E. A., Zidan, N. S., & Aboul-Anean, H. E. D. (2018). The Effect of Nano Materials On Edible Coating and Films' Improvement. *International Journal Of Pharmaceutical Research And Allied Sciences*, 7(3), 20-41.
- Chia, C., Nur, F. R., Mohd, S. S., Sarani, Z., Huang, N., & Lim, H. (2013). Methylene blue adsorption on graphene oxide. *Sains Malaysiana*, 42(6), 819-826.
- Farhan, M. A., Mahmoud, Z. H., & Falih, M. S. (2018). Synthesis and Characterization of TiO<sub>2</sub>/Au Nanocomposite Using UV-Irradiation Method and Its Photocatalytic Activity to Degradation of Methylene Blue. *Asian Journal of Chemistry*, 30(5), 1142-1146. <https://doi.org/10.14233/ajchem.2018.21256>
- Fungaro, D. A., Yamaura, M., & Carvalho, T. E. M. (2014). Adsorption of anionic dyes from aqueous solution on zeolite from fly ash-iron oxide magnetic nanocomposite. *Journal of Atomic and Molecular Sciences*.
- Gan, S., Zakaria, S., Chia, C. H., Chen, R. S., & Jeyalaldeen, N. (2015). Physico-mechanical properties of a microwave-irradiated kenaf carbamate/graphene oxide membrane. *Cellulose*, 22(6), 3851-3863.
- Haciyakupoglu, S., Orucoglu, E., Esen, A. N., Yusan, S., & Erenturk, S. (2015). Kinetic modeling of selenium (IV) adsorption for remediation of contaminated aquatic systems based on meso-scale experiments. *Desalination and Water Treatment*, 56(5), 1208-1216.
- Harja, M., Barbuta, M., Rusu, L., Munteanu, C., Buema, G., & Doniga, E. (2011). Simultaneous removal of astrazone blue and lead onto low cost adsorbents based on power plant ash. *Environmental Engineering & Management Journal (EEMJ)*, 10(3).
- Mahmoud, Z. H., & Khudeer, R. F. Spectroscopy and structural study of Oxidative degradation Congo Red Dye under sunlight using TiO<sub>2</sub>/Cr<sub>2</sub>O<sub>3</sub>-CdS nanocomposite. *International Journal of ChemTech Research*, 12(3) 64-71. DOI: <http://dx.doi.org/10.20902/IJCTR.2019.120311>.
- Mahmoud, Z. H., Falih, M. S., Khalaf, O. E., Farhan, M. A., & Ali, F. K. (2018). Photosynthesis of AgBr Doping TiO<sub>2</sub> Nanoparticles and degradation of reactive red 120 dye. *Journal of Advanced Pharmacy Education & Research/ Oct-Dec*, 8(4).
- Mall, I. D., Srivastava, V. C., & Agarwal, N. K. (2006). Removal of Orange-G and Methyl Violet dyes by adsorption onto bagasse fly ash—kinetic study and equilibrium isotherm analyses. *Dyes and pigments*, 69(3), 210-223.
- Mohan, S. V., Rao, N. C., Prasad, K. K., & Karthikeyan, J. (2002). Treatment of simulated Reactive Yellow 22 (Azo) dye effluents using Spirogyra species. *Waste Management*, 22(6), 575-582.
- Oakes, J., & Dixon, S. (2003). Adsorption of dyes to cotton and inhibition by polymers. *Coloration technology*, 119(3), 140-149.
- Rawnaq, B., Zaid, H., & Farah K. (2018). Evaluation the efficiency of CuFe<sub>2</sub>O<sub>4</sub> prepared photolysis by OSD and photo degradation. *Entomol Appl Sci Lett*, 5(2), 91-100.
- Robinson, T., McMullan, G., Marchant, R., & Nigam, P. (2001). Remediation of dyes in textile effluent: a critical review on current treatment technologies with a proposed alternative. *Bioresource technology*, 77(3), 247-255.
- Soares, G. M., Costa-Ferreira, M., & de Amorim, M. P. (2001). Decolorization of an anthraquinone-type dye using a laccase formulation. *Bioresource Technology*, 79(2), 171-177.
- Sponza, D. T., & Işık, M. (2005). Toxicity and intermediates of CI Direct Red 28 dye through sequential anaerobic/aerobic treatment. *Process Biochemistry*, 40(8), 2735-2744.
- Tavakoli, M. M., Tayyebi, A., Simchi, A., Aashuri, H., Outokesh, M., & Fan, Z. (2015). Physicochemical properties of hybrid graphene-lead sulfide quantum dots prepared by

- 
- supercritical ethanol. *Journal of nanoparticle research*, 17(1), 9:1-13.
- Toor, M., & Jin, B. (2012). Adsorption characteristics, isotherm, kinetics, and diffusion of modified natural bentonite for removing diazo dye. *Chemical Engineering Journal*, 187, 79-88.
- Walker, G. M., Hansen, L., Hanna, J. A., & Allen, S. J. (2003). Kinetics of a reactive dye adsorption onto dolomitic sorbents. *Water Research*, 37(9), 2081-2089.
- Wu, J., Eiteman, M. A., & Law, S. E. (1998). Evaluation of membrane filtration and ozonation processes for treatment of reactive-dye wastewater. *Journal of environmental engineering*, 124(3), 272-277.
- Yousefi, N., Fatehizadeh, A., Azizi, E., Ahmadian, M., Ahmadi, A., Rajabizadeh, A., & Toolabi, A. (2011). Adsorption of reactive black 5 dye onto modified wheat straw: isotherm and kinetics study 1.